University of Bath

Alternative formats

If you require this document in an alternative format, please contact:
openaccess@bath.ac.uk

Polymorph-Selective Deposition of High Purity SnS Thin Films from a Single Source Precursor

Ibbi Y. Ahmet,[†‡] Michael S. Hill,[†] Andrew L. Johnson*[†] and Laurence M. Peter.[†]

[†]Department of Chemistry, University of Bath, Bath, BA2 7AY, United Kingdom.
[‡]Centre for Sustainable Chemical Technologies, University of Bath, Bath, BA2 7AY, United Kingdom.

ABSTRACT: Metal chalcogenide thin films have a wide variety of applications and potential uses. Tin(II) Sulfide, is one such material which presents a significant challenge with the need for high quality SnS, free of oxide materials (e.g. SnO_2) oxides and higher tin sulfides (e.g. Sn2S3 and SnS2). This problem is compounded further when the target material exhibits a number of polymorphic forms with different optoelectronic properties. Unlike conventional chemical vapor deposition (CVD) and atomic layer deposition (ALD), which relies heavily on having precursors that are volatile, stable and reactive, the use of aerosol assisted CVD (AA-CVD) negates the need for volatile precursors. We report here, for the first time, the novel and structurally characterized single source precursor (**1**), Dimethylamido-(N-Phenyl-N',N'-Dimethyl-Thiouriate)Sn(II) dimer, and its application in the deposition, by AA-CVD, of phase-pure films of SnS. A mechanism for the oxidatively controlled formation of SnS from precursor (**1**) is also reported. Significantly, thermal control of the deposition process allows for the unprecedented selective and exclusive formation of either orthorhombic-SnS (α-SnS) or zinc blende-SnS (ZB-SnS) polymorphs. Thin films of α-SnS or ZB-SnS have been deposited onto Mo, FTO, Si and glass substrates at the optimized deposition temperatures of 375 ºC and 300 ºC, respectively. The densely packed polycrystalline thin films have been characterized by XRD, SEM, AFM, Raman spectroscopy, EDS and XPS analysis. These data confirmed the phase purity of the SnS formed. Optical analysis of the α-SnS and ZB-SnS films show distinctly different optical properties with direct band gaps of 1.34 eV and 1.78 eV, respectively. Furthermore photoelectrochemical and external quantum efficiency (EQE) measurements were undertaken to assess the optoelectronic properties of the deposited samples. We also report for the first time the ambipolar properties of the ZB-SnS phase.

Introduction

Precise control over the polymorphism in condensed materials such as semiconductors is of paramount importance.[1] Even small variations in the arrangement of atoms within an extended lattice arrays has a direct effect upon the gap between valence and conduction bands and optical properties of a material, and therefore it's utility in applications such as photovoltaics, photo-catalysis and batteries. While polymorph control in assembled materials such as molecular and polymer based semiconductors[2-4] and in nanocrystalline systems has attracted increasing attention, due to the relative ease by which different polymorphs can be accessed, polymorphic control of semiconducting materials such as metal oxides or chalcogenides is typically only accessible through the application of extreme temperatures and pressures in order to control the bulk phase.

Tin sulphide (SnS) is one such material which possesses a number of polymorphic forms: SnS typically crystallizes in an orthorhombic (*Pnma*) space group (α-SnS,) with *p*-type electrical conductivity and an optimum energy band gap E_g (indirect and direct band gaps at 1.1 eV and 1.3 eV, respectively) that is similar to that of silicon,[5-8] making thin films of α-SnS an attractive, inexpensive, enviromentally benign light harvesting layer in advanced photovoltaic devices. In contrast cubic zinc blende-SnS (ZB-SnS) has a band gap of 1.72-1.76 eV,[8, 9] which has also been applied to the production of photovoltaic devices, although with lower prospective efficiencies.[10] Additional polymorphs of SnS *i.e.* β-SnS (formed at T >800 K)[11, 12] γ-SnS,[13] δ-SnS[14, 15] and rocksalt-SnS (RS-SB, formed at high pressures)[16] have also been reported.

However, despite a Shockley-Queisser limit of 32%, the efficiencies of α-SnS solar cells fall short of their theoretical maximum. Central to recent improvements in device performance has been the control of: i) rigorous purity of phase and stoichiometry (i.e. exclusive production of SnS),[17-19] ii) grain size and control of grain boundary defects[20] and iii) band gap alignment/engineering.[21, 22] While SnS thin films have been grown using a variety of methods, e.g. chemical vapor transport,[23] chemical vapor deposition (CVD),[24-29] chemical bath deposition,[9, 30-33] colloidal nano particle synthesis,[8, 34-38] vacuum evaporation,[6, 17, 39] reactive sputtering,[40]

electrochemical deposition,[14, 41-46] spray pyrolysis,[47, 48] and dip-deposition,[49] in most cases it is challenging to produce phase-pure SnS, as Sn_2S_3 and SnS_2 are often produced in tandem.

Recent advances in the production thin films of SnS, using atomic layer deposition (ALD), have seen an increase in SnS based device efficiencies from 1.3% to 4.6%.[7, 21, 39, 50, 51] Despite its advantages with respect to control of the thin film composition, thickness and conformality, ALD is an expensive, high vacuum and slow process, with challenges to industrial scale-up. In order to prevent the formation of SnS_2 and Sn_2S_3, high deposition temperatures are characteristically needed for CVD (> 400 °C).[25, 28, 29] However, at high temperatures SnS film uniformity is compromised and can deviate from the ideal stoichiometry by 10-20% due to loss of sulfur, which can increase the conductivity of the films to detrimental levels. [7, 17, 25, 29, 50, 52-54] To date, the highest quality thin films of SnS require post deposition treatments, such as sulfurization and hydrogen sulphide annealing, to reduce grain boundary defects, remove secondary phases and lower sulphur vacancies which can act as catalytic sites for recombination.[22a]

Here we report for the first time a simple, practical and scalable single source precursor approach,[55] which provides unmatched oxidation state control, for the deposition of phase-pure SnS. Most notably the variation of temperature in the deposition process allows for the unprecedented and selective formation of thin films of either orthorhombic α-SnS, or cubic ZB-SnS. This is, to the best of our knowledge, the first report of a Sn(II) thio-ureide complex. The novel system is an effective single source precursor, which provides stoichiometric SnS and affords thermal control over the crystalline phase produced (α-SnS or ZB-SnS) during thin film deposition.
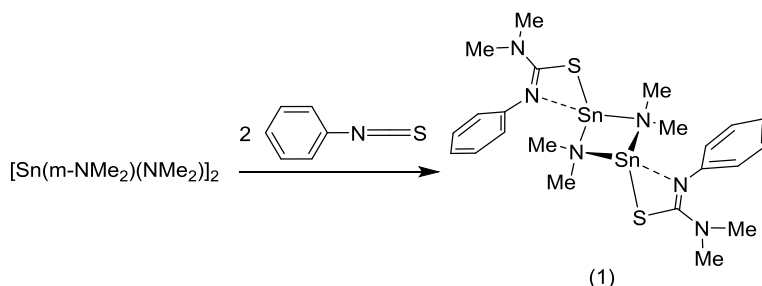
Scheme 1. Synthetic route to the single source precursor (**1**).

While AA-CVD has been used previously in attempts to produce SnS,[24-27] with limited success, previous work in our laboratory has highlighted the utility of iso-ureide Sn(II) complexes as low temperature CVD precursors for Sn(II) oxide thin films.[56] In an attempt to apply this approach to the production of metal sulphide thin films, the stannous thio-ureide, complex 1, was synthesized in high yield by the addition of one molar equivalent of phenyl isothiocyanate to a THF solution of the stannous amide $[Sn(NMe_2)_2]_2$ (Scheme 1)

Results and Discussion

Compound **1** was isolated in effectively stoichiometric yield by crystallization from THF/hexane solutions at -20°C, and characterized by solution state NMR (^1H, ^{13}C and ^{119}Sn) spectroscopy (fig. S8 in SI). Single crystal X-ray diffraction analysis performed on complex 1 revealed the amide bridged dimeric structure shown in figure 1.
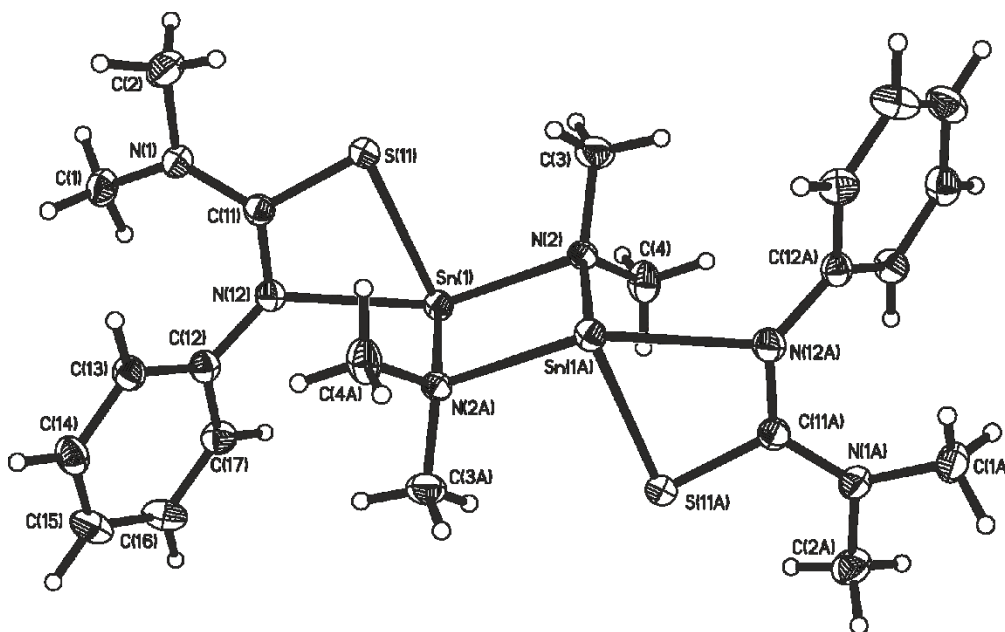
Figure 1. ORTEP diagram (50% probability ellipsoids) of 1. Hydrogen atoms removed for clarity. Sn(1)-S(11) 2.5980(13) Å Sn(1)-N(12) 2.463(4) Å, Sn(1)-N(2) 2.381(4) Å, Sn(1)-N(2A) 2.205(4) Å, C(11)-N(1) 1.353(6) Å; S(11)-C(11)-N(12) 113.9(4)°, S(11)-Sn(1)-N(2) 87.71(10)°, S(11)-Sn(1)-N(2A) 96.53(11)°, N(2)-Sn(1)-N(2A) 80.15(15)°, Sn(1)-N(2)-Sn(1A) 99.85(15)°.

Analysis shows that bidentate $\{k^2\text{-}N,S\text{-Ph-NC(NMe}_2)S\}$ ligands are arranged about the $\{Sn_2N_2\}$ core in a transoidal fashion, with each Sn(II) centre possessing a distorted square pyramidal geometry through a combination of the stereoactive lone pair, bridging amide groups and the bidentate thio-ureide ligand. Significantly, no other examples of Sn(II) thio-ureide complexes have been reported previously. Thermogravimetric analysis (fig. S17 in SI) of **1** shows a single mass loss event with a distinct onset temperature of *ca.* 270 °C. Stable residues were obtained at 314 °C, with a residual mass of ca. 44%, corresponding to the formation of 'SnS'.
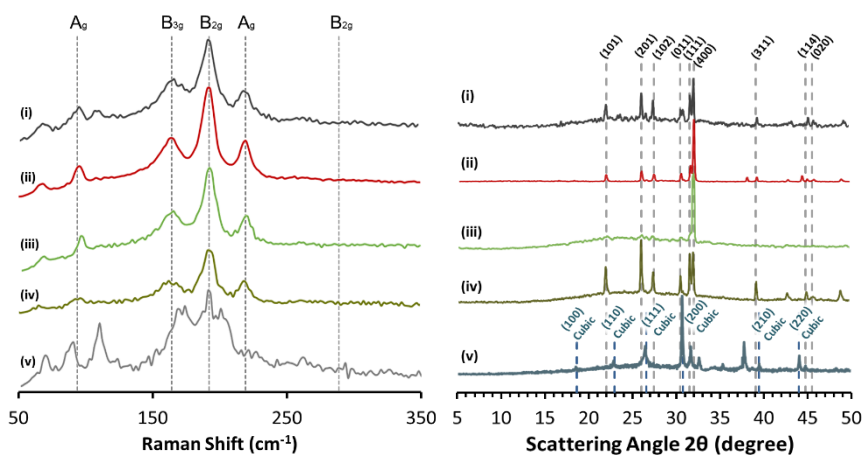
Figure 2. Analysis of SnS films deposited onto glass at (i) 450, (ii) 400, (iii) 375, (iv) 350, and (v) 300 °C for 40 minutes. (left) Raman spectra with assigned symmetry modes for α-SnS[43] and (right) assigned α-SnS (grey) and ZB-SnS (blue) PXRD spectra.

For the first time, black/grey reflective, highly adherent films could be grown by AACVD, from toluene solutions (0.08M) of **1**, with a deposition time of 40 min, onto glass, FTO, Si and Mo substrates, respectively, employing hot wall reactor conditions. Significantly the films were well adhered to substrate and could not be removed by scotch tape. Interestingly, compound **1** has a deposition window between 250 - 500 °C. However, it should be noted that growth rates at either extremes of the temperature range are significantly diminished, resulting in a practical deposition window of between 300-450 °C.

Thin Film Characterization. Using a 532 nm laser, Raman spectroscopy was used to assess the phase purity and lateral uniformity of the SnS films. As seen in figure 2 the Raman spectra of films deposited between 300-450 °C (with 50 °C intervals) and at 375 °C show four distinct characteristic Raman shifts (symmetry modes) at 95 (A_g), 160 (B_{3g}), 190 (B_{2g}) and 218 cm^{-1} (A_g). The observed intense shifts are in full agreement with the Raman spectrum of SnS single crystals [43] and SnS films deposited via ALD.[18] Interestingly, the Raman spectrum for thin films deposited at 300 °C did not show any intense signals and only low intensity peaks were observed at 95, 111, 170 and 195 cm^{-1}. Most significantly, for all samples, no peaks were observed at 307 cm^{-1}, 312 cm^{-1} and 632 cm^{-1}, which are the most intense Raman shifts for Sn_2S_3, SnS2 and SnO2, respectively. This analysis indicates that 1 effectively deposits phase-pure SnS films without secondary phases (Sn_2S_3 and SnS_2) or intrinsic SnO_2 impurities.

Analyses of the films deposited onto silicon substrates were performed using energy-dispersive X-ray spectroscopy (EDS) and the results (fig. S12, SI) for all films the Sn:S ratios is close to 1:1. Table 1 shows the elemental composition of the thin films at various deposition temperatures.

While EDS analysis indicates O and C levels of between 3.3-7.2% and 4.1-7.3% respectively there appears to be no correlation between deposition temperature, however for all samples irrespective of deposition temperature the Sn:S ratio is relatively consistent at around 1:0.95. Examination of the thin films using X-ray photoelectron spectroscopy (XPS) depth profiling experiments reveals these contaminants to be localised on the surface of the thin films: The binding energy of the carbon atoms (C 1s: 284.9 eV) indicates the presence of organic hydrocarbon contaminates, and significantly the absence of intrinsic tin carbide environments (e.g. C 1s: 282.9 eV in Nb_2SnC).[57] In the case of oxygen, XPS analysis highlights a small degree of surface oxidation of the SnS, as indicated by the distinctive peaks at 486.9 eV (Sn 3d5/2) and 495.3 eV (Sn 3d3/2), which are representative of SnO_2 binding energies (fig. S14 SI).[40] Depth profiling of the thin films (20 s Ar etch) shows a disappearance of peaks associated with hydrocarbon based carbon (C 1s: 284.9 eV), and a decrease in intensity of the O 2s peak (531.5 eV).This occurs simultaneously with a decrease in the Sn 3d peaks at 486.9 and 495.3 eV (i.e SnO_2 peaks), and an increase of the intensity of the Sn 3d peaks at 486.5 (Sn 3d5/2) and 495.1 eV (Sn 3d1/2), indicative of the SnS binding energies.

Furthermore the S peaks at 162.6 (S 2p1/2) and 161.0 eV (S 2p3/2) associated with SnS is observed before and after etching (fig. S16 SI). Further etching (200 s Ar etch) of the samples shows a loss of the surface oxide material to reveal SnS, as indicated by the averaged elemental ratio of Sn:S of 1:0.95 (fig. S14-15 SI). Similar XPS studies of SnS films have shown comparable atomic ratios for "pure SnS" as well as surface of oxidation.[29, 40, 43]

Table 1. Elemental composition of films deposited at various temperatures from EDS analysis. (Full EDS Spectrum can be found in the Supporting Information Fig S12 b-f)†

Precursor (1)	Sn:S	C (atm %)	O (atm %)
300 °C	1:0.94	7.30 %	4.7 %
350 °C	1:1.00	4.13 %	4.5 %
375 °C	1:0.96	6.4 %	7.2 %
400 °C	1:0.95	4.6 %	3.3 %
450 °C	1:0.87	6.3 %	4.3 %

† EDS measurement were taken from several positions (10 points) over the sample in order to show homogeneity of the thin film samples and the numbers presented in Table 1 are the averages of those findings.

Although scanning electron micrographs of SnS films grown onto Si substrates at 400 °C and 350 °C for 40 min show crystallite growth, both films appear to have incomplete surface coverage. Optimum deposition conditions, with respect to the formation of compact uniform films, was found to be at 375 °C, and micrographs of these films show the presence of large triangular grains (~500 nm) with a uniform film thickness of 800 nm. As is apparent from inspection of Figure 3, all of the thin films are highly crystalline and highly orientated.

In the case of thin films grown at 375 °C, the crystallites grow up from the substrate from their smallest crystal dimension. Significantly, the morphology of the films deposited at 300 °C (40 mins) differs considerably from those deposited at either 400, 375 or 350 °C, which consist of compact interpenetrating cube-like crystallites of relatively uniform size and dimension (500-600 nm). AFM

analysis of the films (fig. 4) deposited at 375 °C and 300 °C, clearly shows a significant difference in the film roughness. PXRD analysis of the films deposited at 450, 400, 375, and 350 °C shows the presence of diffraction peaks consistent with the formation of orthorhombic, α-SnS.[58]
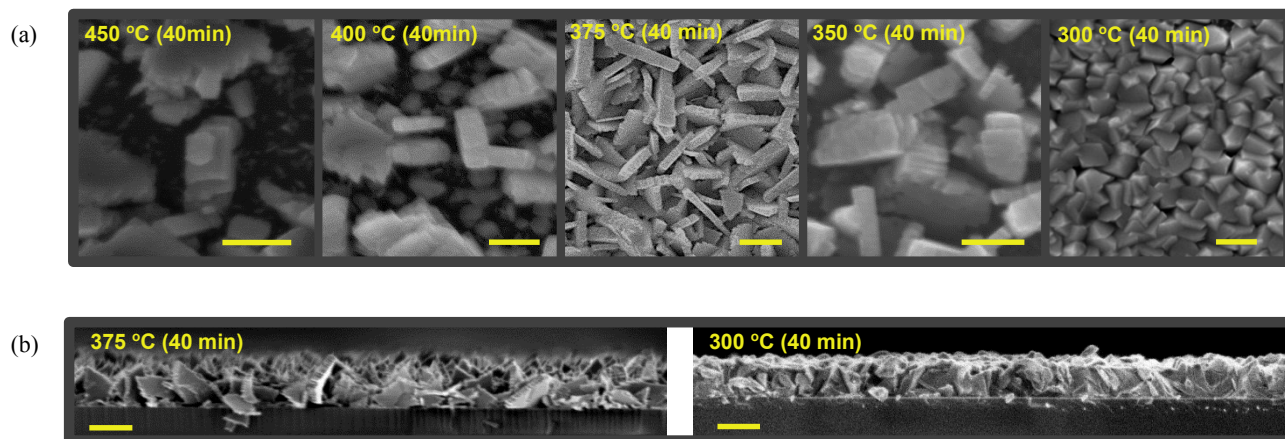
Figure 3. (a) Top down SEM micrographs of thin films grown at 450, 400, 375, 350 and 300 °C, respectively, onto (100) silicon wafers (b) Cross-section micrographs of SnS films grown at 300 and 375 °C (40 mins) (Scale bar = 500 nm)
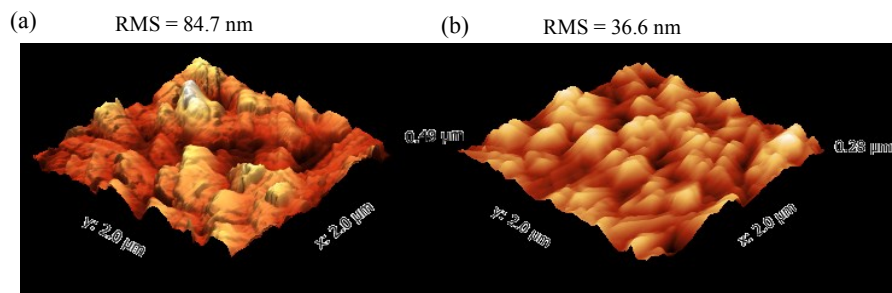

Figure 4. AFM 3D surface plot of SnS film grown at 375 °C (a) and 300 °C (b).

Figure 2 shows the PXRD patterns of films deposited onto glass at five different temperatures; while films deposited at 450, 400 and 350 °C all display peaks associated with reflections from the [1,0,1], [2,0,1], [1,0,2], [1,1,1] and [4,0,0] planes, films deposited at 375 °C show only a single intense reflection arising from the [4,0,0] plane, suggesting a highly orientated material; an observation supported by SEM analysis. Similarly highly orientated SnS films have been reported from ALD[18] and nano-ink deposition processes.[36] Additionally, the films grown onto glass and crystalline silicon at 375 °C (i.e. α-SnS), are highly orientated, showing a single peak for the [4,0,0] plane. To observe preferential orientation in non-cubic materials such as SnS, which possess an orthorhombic crystal structure, is not uncommon. This observation can be a consequence of high deposition rates (c.a. 17 nm/min) at 375 °C, coupled with anisotropic growth rates in layered systems such as α-SnS.[59]

Films grown onto FTO and Mo, are less orientated (fig. S22 SI). The PXRD analysis for films deposited at 300 °C only produces peaks corresponding to the cubic phase of SnS with a lattice parameter of a = 5.846 Å (ZB-SnS)[8, 9, 31, 34, 35, 38, 51, 60] (i.e. [1,0,0], [1,1,0], [1,1,1], [2,0,0] and [2,2,0] planes). Only the peak in the ZB-SnS thin film, at 2θ = 37.5 °, could not be identified and assigned a specific miller index. However the same peak has been identified (and not assigned) in the PXRD pattern of ZB-SnS nanocrystals synthesised by Deng et al.[35] Interestingly, ZB-SnS has previously been identified as thermodynamically unstable *cf* α-SnS.[61] However, these films are evidently kinetically stable; ZB-SnS films show no evidence of spontaneous conversion to α-SnS at room temperature. At elevated temperatures (i.e. 375 °C) ZB-SnS films show a phase transition from ZB-SnS to α-SnS over a period of 5hrs under N_2 (fig. S21, SI) as evidenced by PXRD analysis.[8, 51]

Decomposition Mechanism. In an attempt to fully understand the mechanism by which precursor **1** produces phase-pure SnS materials we examined the gaseous by-products from an AA-CVD run at 375 °C. Gaseous by-products were trapped at low temperature (77 K) from the CVD chamber exhaust (see Fig. S1 SI). The condensed gaseous by-products consisted of a clear solution, which was then vacuum evaporated until a white residue remained. The remaining residue was dissolved in THF-d^8 and examined by ^{1}H and ^{13}C NMR Spectroscopy (see Fig. S9 SI) from which were able to identify that the phenyl guanidine compound was formed as a by-product from the decomposition of precursor **1**.
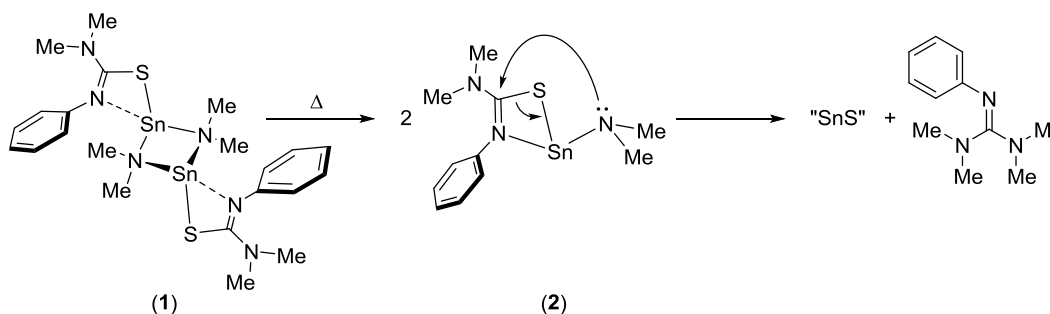
Scheme 2. Possible mechanism for the formation of SnS and *N,N,N',N'*-tetramethyl-*N"*-phenyl-guanidine from precursor (1).

Evidence form high temperature (323 K) ^{119}Sn NMR studies suggests that at elevated temperatures the dimer complex (**1**), identified in the solid state (figure 1) breaks down into the monomeric species (**2**), which we assume facilitates SnS formation via the nucleophilic attack of {NMe$_2$} groups at the central carbon atom of the thio-ureide ligand. While we have no direct evidence for an intramolecular reaction mechanism, this seems most plausible.

Optical Analysis. The optical absorption behaviour of the SnS films was determined by optical transmission measurements. The optical transmission spectra of 800 nm thick SnS film of both α-SnS and ZB-SnS deposited onto glass substrates is shown in the supporting information (Fig. S18a SI). For α-SnS thin films, absorption coefficients were calculated to be above 4 x 10^4 cm^{-1}, at wavelengths below 800 nm. Interesting, the ZB-SnS has an absorption coefficient above 4 x 10^4 cm^{-1}, at wavelengths below 595 nm. The optical band gaps for both materials were determined from Tauc plots of the absorption spectra (Fig. S18c-d SI); α-SnS films were calculated to have direct and indirect band gaps of 1.34 eV and 1.10 eV respectively, which corresponds closely to previously reported values for 500 nm α-SnS films deposited by ALD.[18]

Films of ZB-SnS are found to have a direct band gap of 1.78 eV, which is at a higher energy compared to previously reported ZB-SnS containing films (1.76-1.68eV).[8-10]

Photoelectrochemical Analysis. Photoelectrochemical measurements under a chopped illumination (470 nm) were performed on α-SnS and ZB-SnS films deposited on Mo/glass-substrates. Figure 5 shows the photoelectrochemical behaviour of the different SnS films across the potential range from -0.7 V to +0.7 V vs. Ag|AgCl. For the α-SnS films, only cathodic photo-currents are seen on the scan, demonstrating *p*-type conductivity. The photocurrent increases with increasing cathodic polarization, as a result of increased band bending.

By contrast, the ZB-SnS films exhibit both cathodic and anodic photocurrent responses of similar magnitude with a cross-over close to the estimated flat band potential, E$_{fb}$ for ZB-SnS (-0.13 V). ZB-SnS has previously been reported to be an extrinsic *p*-type semiconductor,[9] however, as can be seen in figure 5a, the ZB-SnS exhibits ambipolar photocurrent behaviour, suggesting that the ZB-SnS material may be compensated. Interestingly, previous work by Rat et al, report similar ambipolar photoelectrochemical behaviour from the SnS thin films they deposited via spray pyrolysis methods. It was speculated that the presence of both anodic and cathodic photocurrents was a result of a mixture of p-type and n-type semiconducting phases of SnS through mixed-stoichiometry in the SnS system.[62] However, in our investigation we have identified that the ambipolar photoelectrochemical behaviour is attributed to the electrical properties the ZB-SnS phase.
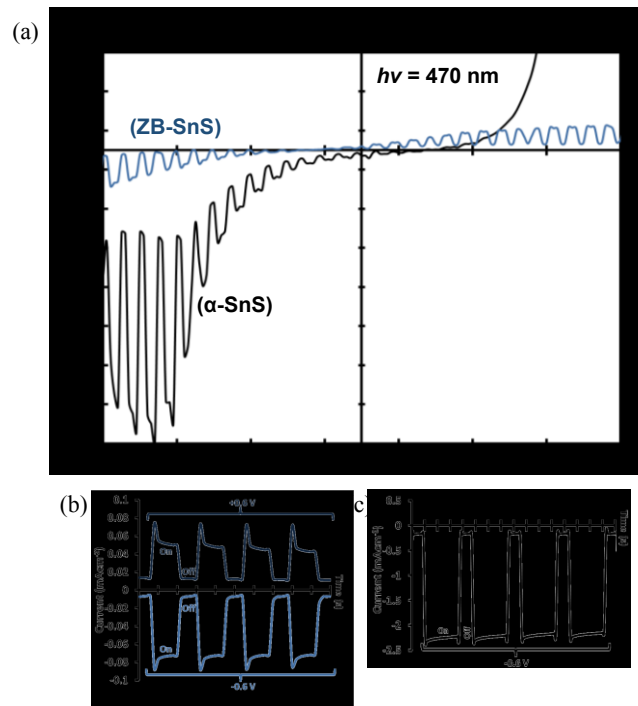
Figure 5. Photo-electrochemical responses (vs. Ag|AgCl) to chopped illumination (1 s on, 1 s off) in a 0.2 M Eu$^{2+/3+}$(aq) electrolyte of ZB-SnS (blue) and α-SnS (black) films (on Mo/glass). Reference electrode Ag|AgCl. (a) Voltage sweep from +0.7 V to -0.7 V for the two samples. (b) Transient photocurrent for ZB-SnS at fixed potentials, +0.6V (dark blue) and -0.6 V (blue) and (c) α-SnS at a fixed potential of -0.6V (black).

EQE Measurements. As shown in figure 6, the EQE spectrum for α-SnS, shows an onset at 1100 nm and a step at 900 nm, which correspond respectively to the indirect and direct band gap transitions observed in the optical analysis. The EQE reaches 43-53 % between 780-400 nm, which is remarkably high for an as-deposited and untreated/un-annealed thin film. ZB-SnS films on Mo produced two different EQE spectra dependent on the sign of the photocurrent. At a bias potential of -0.7 V (cathodic), a sharp photocurrent onset was observed at 760 nm close to the band gap energy. The EQE then peaks at 30% at a wavelength of 675 nm, before decreasing steadily at shorter wavelengths. By contrast, at a bias potential of +1.0 V (anodic), the EQE spectrum shows a more gradual onset at 770 nm followed by a step at 720 nm and a steady increase towards shorter wavelengths, reaching 15 % at 400 nm. The difference in the spectra indicates that the mechanism of photocurrent generation in the two cases is different. Under an anodic photocurrent, the peak in the spectrum close to the band edge is typical for photoconductivity, which is a bulk effect in which photogenerated charge carriers increase the conductivity of a material. In contrast, the EQE spectrum for the cathodic photocurrent is more typical of a photovoltaic effect in which charge carriers are separated in the space charge region formed at the semiconductor-electrolyte junction.

For both thin films, short circuit current densities (J_{sc}) have been calculated under AM 1.5 G illumination, assuming the photocurrent and light intensity follow a linear relationship.[63] The values obtained are for an 800 nm thick α-SnS J_{sc} (+1.0 V) = 15.58 mA cm^{-2}; 600 nm thick ZB-SnS J_{sc} (+1.0 V) = 2.19 mA cm^{-2}, and J_{sc} (-0.7 V) = 4.13 mA cm^{-2}. The J_{sc} for α-SnS is comparable with the best SnS device reported to-date.[17]

Our findings suggest the thin films of both α-SnS and ZB-SnS are exceedingly stable. Despite initial surface oxidation of the thin films post deposition, as revealed by XPS analysis, the samples are stable to wetting and successive testing. Even after 9 months of storage in air, samples of the thin films show identical EQE spectra to week old samples, suggesting a high degree of durability to both the materials and any subsequent device that may be fabricated from them.
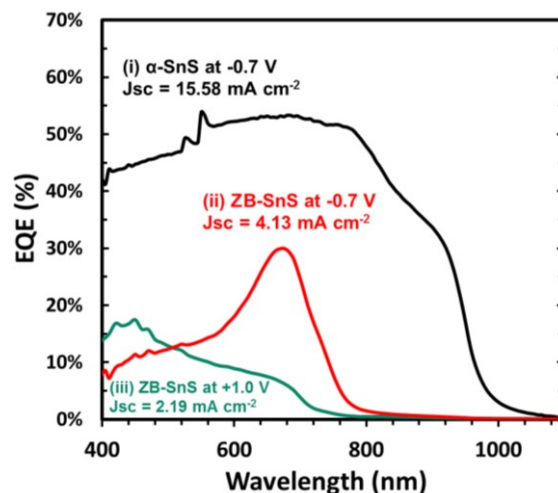
Figure 6. EQE Spectrum of **(i)** α-SnS at -0.7 V, **(ii)** ZB-SnS at -0.7 V and **(iii)** ZB-SnS at +1.0 V (vs. Ag|AgCl)

Conclusion

In summary, we present the first example of a tin thio-ureide complex, capable of producing high purity SnS thin films. In addition, temperature control in the deposition process allows for the exclusive formation of thin films of either orthorhombic α-SnS, or cubic ZB-SnS. Our work demonstrates that the novel stannous thio-ureide complex, **1**, holds the potential for the production of α-SnS based thin films on a commercial scale using a low-cost deposition technology (AACVD). Additionally, the potential dependent photoelectrochemical properties of phase-pure thin films of metastable ZB-SnS have been characterized for the first time. The identification of the p- and n-type photocurrent behaviour within the ZB-SnS phase can assist in the development of SnS photovoltaic devices. An absorber layer with a mixture of SnS polymorphs can have a significantly detrimental effect on the α-SnS device performance. Therefore it will be important for future α-SnS device optimization to identify exact polymorph present within the film. We are now in the process of developing both α-SnS and ZB-SnS based solar cells and will publish these findings at a later point.

In addition, through the fine tuning of the thio-ureide system we have begun to explore a wide range of novel precursors capable of selectively depositing a choice of desirable metal chalcogenide thin films with comparable control over phase purity and polymorphism. Such control over the selective deposition of phase-pure samples is the first step in the development of a thin film materials database and structural property maps, ultimately guiding the appropriate thin film selection for specific engineering applications.

Experimental Section

General Techniques:

All reactions were carried at using the standard Schlenk line and glove box techniques under an inert atmosphere of argon and nitrogen, respectively. Tetrahydrofuran (THF) was dried over potassium before isolating via distillation. Hexanes and toluene solvents were dried using a commercially available solvent purification system (Innovative Technology Inc., MA) and all solvents degassed under argon prior to use. Deuterated benzene (C_6D_6) and deuterated THF (THF-d^8) NMR solvent was purchased from Fluorochem, UK, and dried over potassium before isolating via vacuum distillation. All dry solvents were stored under argon in Young's ampoules over 4 Å molecular sieves. All reagents were purchased from Sigma-Aldrich and used as supplied. The starting materials, phenylthioisocyanide was purchased from Aldrich Chemicals, and tetrakis(dimethylamido)ditin(II) was synthesized according to literature procedure. [64, 65]

NMR experiments: NMR Experiment were conducted in Young's tap NMR tubes, prepared and sealed in a glove box with an argon atmosphere. For all experiments THF-d^8 was used as the NMR solvent. NMR data was collected at 25 $^{\circ}$C either using a Bruker AV-300 spectrometer operating at 300.22 MHz (^{1}H), 75.49 MHz (^{13}C) and 111.95 MHz (^{119}Sn) or a Bruker AV-500 spectrometer at 111.95 MHz (^{119}Sn). Chemical shifts were given in ppm and referenced internally to residual non-deuterated solvent resonances. The following abbreviations are used: s (singlet), t (triplet), q (quartet), m (multiplet) and b (broad). [66]

Melting Point Analysis: Grinded powdered compound was placed inside glass capillary tube under an atmosphere of argon and melting points were determined using a Stuart SMP10 Melting Point Apparatus.

Elemental analyses: Elemental analyses were performed externally by London Metropolitan University Elemental Analysis Service, UK.

Single Crystal X-ray Diffractometry: Single X-ray crystallography data was collected at 150 K on Nonius Kappa CCD diffractometers equipped with low temperature devices, using graphite monochromated Mo-Kα radiation (λ = 0.71073 Å). The data collected by the diffractometers was processed using the Nonius Software. Structure solution, followed by full-matrix least squares refinement was performed using either the WinGX-170 suite of programs or the programme suite X-SEED. Crystals were isolated from argon filled Schlenks and immersed under oil before mounted onto the diffractometer.

Full crystallographic data for compound (**1**) is included in the supporting information.

Substrate Preparation: Polycrystalline Molybdenum (Mo) (110 oriented) substrates were sputter coated onto 0.5 mm soda lime glass slides (~ 4 nm Rms) and purchased from MTI corporations, Tec 7(~7Ω/cm^2) Flourine doped Tin Oxide (FTO, 101 oriented) on glass substrates (~ 20 nm Rms) were purchased from Sigma-Aldrich, P-type boron doped 100 oriented silicon wafers were supplied by Element 6™ (~ 1 nm Rms) and 5mm High Grade float--glass substrates were coated with a 20 nm layer of crystalline NaSiO$_2$ and purchased from Pilkington (~ 1 nm Rms). Glass, FTO and Silicon substrates were cleaned using a dilute solution (2%) of Hemanex™ in 1:1 iso-propanol and deionised water. The films were then cleaned with a 0.3 M solution of Acetic acid in isopropanol, then isopropanol and finally dried under a fast flow of N$_2$. Glass and FTO substrates were further cleaned using a low pressure O$_2$ plasma reactor for 15 minutes (This increases the surface wetting). Mo substrate were cleaned in a bath of 20% ammonium hydroxide solution for two hours then washed with deionised water and isopropanol. All substrates were wiped with dried lint free clothes before deposition to remove possible dust particles on the surface.

Aerosol Assisted Chemical Vapour Deposition (AA-CVD) procedure: The precursor solution is prepared within a glove box under an atmosphere of argon and all solvents are dried and degassed prior to preparation. The precursor holder is kept under an atmosphere of argon, sealed and attached onto to the AA-CVD apparatus. Once all substrates were prepared and mounted into the deposition chamber, argon gas is allowed to flow through the system, bi-passing the precursor holder, for 20 minutes in order to purge the system with argon. Then with continuing gas flow the hot-wall furnace is switched on and allowed to reach the target deposition temperature and equilibrate for 20 minutes. Once this is achieved the gas flow is diverted to flow via the precursor solution which draws the solution into the TSI 3076 Constant Output Atomiser and out into the deposition chamber where the deposition commences and the timer is started. Gas flow is monitored via bubbler and gas pressure fixed 10 bar until it reaches the atomiser. A diagram of the AA-CVD apparatus is included in the supporting information.

UV-Vis-IR spectroscopy measurements: UV-Vis-IR spectroscopy measurements were collected using a PerkinElmer® LAMBDA 750/650 UV/Vis & UV/Vis/NIR Spectrophotometer. Measurements were recorded at 2000 to 400 nm and zero referenced using 5mm High Grade Pilkinton Float-glass substrates. The measurements were recorded with 1 nm increments. At 860 nm the PbS detector switches over to the Photo Multiplier Detector (PMD), as a result the a small stepwise noise is generated (±10 nm) within the raw data spectrum.

Thermogravimetric Analysis (TGA): TGA was collected using a TGA 4000 Perkin Elmer system. Samples were prepared air sensitively using a crimped aluminium sample pan. TGA's were performed under a flow of N$_2$ at 20 ml min^{-1} and heated from 30 °C to 600 °C at a ramp rate of 5 °C min^{-1}.

Powder X-ray Diffractometry (PXRD): PXRD data was collected on a BRUKER D8-Advance. The X-ray diffraction spectra were collected for the thin films using the flat plate mode from 5 to 70 2θ at 2° per minute. X-rays were generated from a Cu source at wave lengths of 1.54 Å.

Scanning Electron Microscopy (SEM): SEM was performed to visualize the morphology of the films both as cross sections (using a Field Emission Scanning Electron Microscope 6301F) and top down (JEOL 6480 Low Vacuum large stage SEM platform) images. The films were prepared by mounting onto steal SEM mounts with conductive carbon tape attached to the bottom and top surface of the films, to maximize conductivity of electrons and prevent charge accumulation. Samples were desiccated at 35 °C for 24 hour prior analysis.

Atomic Force Microscopy (AFM): AFM analysis was performed using a Digital Instruments Nanoscope IIIa, with BRUKER SNL-10 Silicon on Nitride Lever contact tips (tip radius <10 nm, f$_0$: 50-80 kHz, k: 0.350 N/m and T: 600nm), in contact mode. Images processed using the open access Gwyddion SPM data analyzer.

Energy dispersive X-ray spectroscopy (EDS): EDS was performed using Oxford Instruments Scanning Electron Microscope 6480 LV and processed on INCA Wave software. All spectrums were standardized and calibrated against a standard silicon wafer sample. The magnification, working distance and beam energy (10 keV) were kept consistent between spectral analyses.

X-ray photoelectron spectroscopy (XPS): XPS was performed at NEXUS nanoLAB facilities at the University of Newcastle. All spectra were collected using a Theta Probe Angle-Resolved X-ray Photoelectron Spectrometer (ARXPS) System by Thermo Scientific and processed using CasaXPS software. X-rays were generated from a high power monochromated Al Kα source with spot size 15 μm and spectra calibrated to carbon 1s bond energy of 284 eV. For etching an Argon gas cluster ion source was used with a 4 KeV (1000 atoms/cluster) with raster size of 1 mm x 2 mm and X-ray spot size of 150 μm radius / 70,650 μm^2.

Raman Spectroscopy: Raman spectra were collected using a Renishaw inVia Raman Microscope fitted with a 532 nm laser at a 10 % spot size, 3 s exposure time and 1 % energy intensity. The data was processed using a Renishaw WiRE software package.

Photoelectrochemical measurements: (Detailed Experimental set-up can be found in the SI) For all photo electrochemical measurement only two samples deposited onto Mo/Glass substrates were used, which consisted of either α-SnS (800nm) deposited 375 °C for 40 mins or ZB-SnS (600 nm) deposited at 300 °C for 40 mins. All photo electrochemical measurements were undertaken in a aqueous solution of 0.2 M Eu(NO$_3$)$_2$ at pH 7. The three electrode electrochemical cell was placed in a Faraday cage during measurements and was made up of an Ag│AgCl reference electrode, a Pt counter electrode and the working electrode acting as the sample. The sample was placed so that the deposited sample surface is directed towards the incident light without shadowing of the other two electrodes. The transient photocurrents were recorded using a pulsed 470 nm LED illumination (on for 1 s and off for 1 s) with a sweeping potential from -0.7 V to +0.7 V at 0.02 V per second. Using the same 470 nm LED chronoamperometry measurements were conducted at fixed potentials of -0.6 V or +0.6 V with a light pulse of 1.5 sec on and 0.5 sec off, with an equilibrium time of 30 seconds. (Detailed Description of the EQE measurements can be found in the SI) Photocurrent spectra of both samples were conducted in the same three electrode electrochemical cell. The variable wavelength incident light was provided by tungsten lamp and grating

monochromator. The incident light was chopped at 27 Hz, and a lock-in amplifier (Stanford Research Systems) was used to detect the photocurrent. Measurements of the photocurrent as a function of wavelength were made at a potential of -0.7 V or +1.0 V vs. Ag|AgCl, using a DC power supply. Measurements in the range 1100-400 nm were performed with 10 nm intervals. In order to obtain the external quantum efficiency (EQE) of the SnS films, the incident photon flux was calibrated using standardized 1 cm^2 Si photo-diode traceable to NBS standards. The after all EQE measurements photo current measurements as a function of wavelength were recorded using the Si photodiode in order to calibrate the spectral flux produced by the tungsten lamp, which is used in the calculations of the EQE. Detailed description of the method used to calculate the EQE from the photocurrent spectra is presented in the SI.

Synthesis of Dimethylamido-(N-Phenyl-N',N'-Dimethyl-Thiouriate)Sn(II) dimer [Sn({C₆H₅}NCSN{Me₂})(NMe₂)] Compound (1): Phenylisothiocyanate (2.40 ml, 2.276 g, 20.10 mmol) was added drop wise, over 10 minutes, to a cooled (-40 °C) and stirred THF solution (100 ml) of tetrakis(dimethylamido)ditin(II) (4.180 g, 20.10 mmol) which resulted in an instantaneous colour change from yellow to colourless. After stirring at room temperature for 2 hrs, THF was removed *in-vacuo*. To the residual solid 80 ml of hexane was added and stirred for 1 hour, where-upon a white precipitate evolved. The hexane was removed from the precipitate by cannula filtration. The precipitate was washed a further two times with fresh hexane. The white precipitate was then dissolved in a THF:hexane mix (15ml:30 ml). After filtration through celite, the solution was stored at -20 °C for 3 days, during which time colourless crystalline needles were formed. The product was subsequently isolated by filtration and dried *in-vacuo*. Yield 5.552 g, 86 % , m.p. 125 °C decomposed to black. Analysis, found (calc. for $C_{11}H_{17}N_3SSn$): C 38.40 (38.63); H 5.35 (5.01); N 12.15 (12.29). ^{1}H NMR (300 MHz, THF-d^8): δ_H 7.20-7.11 (m, 2H, N(C₆H₅)), 6.91-6.72 (m, 3H, N(C₆H₅)), 2.83 (s, 6H, N(CH₃)), 2.62 (s, 6H, N(CH₃)).^{13}C NMR (75.5 MHz, THF-d^8): δ_C 129.43 (s, N-C(=S)-N),123.23 (s, N(C₆H₅)), 45.37 (s, N(CH₃)), 42.13 (s, N(CH₃)). ^{119}Sn NMR (111.95 MHz, THF-d^8): δ_{Sn} 38.50 (s).

Associated Content

Supporting Information

A Photographic image and ^{1}H, ^{13}C, ^{119}Sn NMR data of compound (**1**) can be found in figures S7-8 (in the SI). X-ray crystallographic files in CIF format for the structure determinations for compound (**1**) is provided. Additional SEM images are also provided. CCDC 1417256 contains the supplementary crystallographic data for this paper. These data can be obtained free of charge from The Cambridge Crystallographic Data Centre via www.ccdc.cam.ac.uk/data_request/cif.

REFERENCES

(1) Buckeridge, J.; Butler, K. T.; Catlow, C. R. A.; Logsdail, A. J.; Scanlon, D. O.; Shevlin, S. A.; Woodley, S. M.; Sokol, A. A.; Walsh, A., Polymorph Engineering of TiO2: Demonstrating How Absolute Reference Potentials Are Determined by Local Coordination. *Chem. Mater.,* **2015,** 27, 3844-3851.

(2) Hiszpanski, A. M.; Baur, R. M.; Kim, B.; Tremblay, N. J.; Nuckolls, C.; Woll, A. R.; Loo, Y.-L., Tuning Polymorphism and Orientation in Organic Semiconductor Thin Films via Post-deposition Processing. *J. Am. Chem. Soc.,* **2014,** 136, 15749-15756.

(3) Salammal, S. T.; Balandier, J.-Y.; Arlin, J.-B.; Olivier, Y.; Lemaur, V.; Wang, L.; Beljonne, D.; Cornil, J.; Kennedy, A. R.; Geerts, Y. H.; Chattopadhyay, B., Polymorphism in Bulk and Thin Films: The Curious Case of Dithiophene-DPP(Boc)-Dithiophene. *J. Phys. Chem. C.,* **2014,** 118, 657-669.

(4) Stevens, L. A.; Goetz, K. P.; Fonari, A.; Shu, Y.; Williamson, R. M.; Brédas, J.-L.; Coropceanu, V.; Jurchescu, O. D.; Collis, G. E., Temperature-Mediated Polymorphism in Molecular Crystals: The Impact on Crystal Packing and Charge Transport. *Chem. Mate.* **2015,** 27, 112-118.

(5) Parenteau, M.; Carlone, C., Influence of temperature and pressure on the electronic transitions in SnS and SnSe semiconductors. *Phys. Rev. B,* **1990,** 41, 5227-5234.

(6) Devika, M.; Ramakrishna Reddy, K. T.; Koteeswara Reddy, N.; Ramesh, K.; Ganesan, R.; Gopal, E. S. R.; Gunasekhar, K. R., Microstructure dependent physical properties of evaporated tin sulfide films. *J. Appl. Phys.,* **2006,** 100, 023518.

(7) Ramakrishna Reddy, K. T.; Koteswara Reddy, N.; Miles, R. W., Photovoltaic properties of SnS based solar cells. *Sol. Energ. Mater. Sol. C.* **2006,** 90, 3041-3046.

(8) Greyson, E. C.; Barton, J. E.; Odom, T. W., Tetrahedral Zinc Blende Tin Sulfide Nano- and Microcrystals. *Small,* **2006,** 2, 368-371.

(9) Avellaneda, D.; Nair, M. T. S.; Nair, P. K., Polymorphic Tin Sulfide Thin Films of Zinc Blende and Orthorhombic Structures by Chemical Deposition. *J. Electrochem. Soc.,* **2008,** 155, D517-D525.

(10) Garcia-Angelmo, A. R.; Romano-Trujillo, R.; Campos-Álvarez, J.; Gomez-Daza, O.; Nair, M. T. S.; Nair, P. K., Thin film solar cell of SnS absorber with cubic crystalline structure. *Phys. Status Solidi,* **2015,** 1-9.

(11) Chattopadhyay, T.; Pannetier, J.; Von Schnering, H. G., Neutron diffraction study of the structural phase transition in SnS and SnSe. *J. Phys. Chem. Solids,* **1986,** 47, 879-885.

(12) Vonschnering, H. G.; Wiedemeier, H., The High-Temperature Structure of Beta-Sns and Beta-Snse and the B16-to-B33 Type Lambda-Transition Path. *Z. Kristallogr.,* **1981,** 156, 143-150.

(13) Ehm, L.; Knorr, K.; Dera, P.; Krimmel, A.; Bouvier, P.; Mezouar, M., Pressure-induced structural phase transition in the IV-VI semiconductor SnS. *J. Phys. Condens. Mat.,* **2004,** 16, 3545-3554.

(14) Brownson, J. R. S.; Georges, C.; Larramona, G.; Jacob, A.; Delatouche, B.; Levy-Clement, C., Chemistry of tin monosulfide (δ-SnS) electrodeposition effects of pH and temperature with tartaric acid. *J. Electrochem. Soc.,* **2008,** 155, D40-D46.

(15) Brownson, J. R. S.; Georges, C.; Lévy-Clément, C., Synthesis of a δ-SnS Polymorph by Electrodeposition. *Chem. Mater.,* **2006,** 18, 6397-6402.

(16) Mariano, A. N., Polymorphism in Some Iv-Vi Compounds Induced by High Pressure and Thin-Film Epitaxial Growth. *Appl. Phys. Lett.,* **1967,** 10, 282.

(17) Steinmann, V.; Jaramillo, R.; Hartman, K.; Chakraborty, R.; Brandt, R. E.; Poindexter, J. R.; Lee, Y. S.; Sun, L.; Polizzotti, A.; Park, H. H.; Gordon, R. G.; Buonassisi, T., 3.88% Efficient Tin Sulfide Solar Cells using Congruent Thermal Evaporation. *Adv. Mater.,* **2014,** 26, 7488-7492.

(18) Sinsermsuksakul, P.; Heo, J.; Noh, W.; Hock, A. S.; Gordon, R. G., Atomic Layer Deposition of Tin Monosulfide Thin Films. *Adv. Energ. Mater.,* **2011,** 1, 1116-1125.

(19) Kim, J. Y.; George, S. M., Tin Monosulfide Thin Films Grown by Atomic Layer Deposition Using Tin 2,4-Pentanedionate and Hydrogen Sulfide. *J. Phys. Chem. C,* **2010,** 114, 17597-17603.

(20) Hartman, K.; Steinmann, V.; Jaramillo, R.; Chakraborty, R.; Park, H. H.; Leizhi, S.; Brandt, R. E.; Yun Seog, L.; Gordon, R. G.; Buonassisi, T. In *Impact of H₂S annealing on SnS device performance*, Photovoltaic Specialist Conference (PVSC), 2014 40th IEEE, 0362-0364.

(21) Sun, L.; Haight, R.; Sinsermsuksakul, P.; Bok Kim, S.; Park, H. H.; Gordon, R. G., Band alignment of SnS/Zn(O,S) heterojunctions in SnS thin film solar cells. *Appl. Phys. Lett.* **2013,** 103, 181904.

(22) Burton, L. A.; Walsh, A., Band alignment in SnS thin-film solar cells: Possible origin of the low conversion efficiency. *Appl. Phys. Lett.* **2013,** 102, 132111.

(23) Burton, L. A.; Colombara, D.; Abellon, R. D.; Grozema, F. C.; Peter, L. M.; Savenije, T. J.; Dennler, G.; Walsh, A., Synthesis, Characterization, and Electronic Structure of Single-Crystal SnS, Sn₂S₃, and SnS₂. *Chem. Mater.,* **2013,** 25, 4908-4916.

(24) Bade, B. P.; Garje, S. S.; Niwate, Y. S.; Afzaal, M.; O'Brien, P., Tribenzyltin(IV)chloride Thiosemicarbazones: Novel Single Source Precursors for Growth of SnS Thin Films. *Chem. Vapor Depos.,* **2008,** 14, 292-295.

(25) Kevin, P.; Lewis, D. J.; Raftery, J.; Azad Malik, M.; O'Brien, P., Thin films of tin(II) sulphide (SnS) by aerosol-assisted chemical vapour deposition (AACVD) using tin(II) dithiocarbamates as single-source precursors. *J. Cryst. Grow.,* **2015,** 415, 93-99.

(26) Parkin, I. P.; Price, L. S.; Hibbert, T. G.; Molloy, K. C., The first single source deposition of tin sulfide coatings on glass: aerosol-assisted chemical vapour deposition using [Sn(SCHCHS)]. *J. Mater. Chem.,* **2001,** 11, 1486-1490.

(27) Price, L. S.; Parkin, I. P.; Hibbert, T. G.; Molloy, K. C., Atmospheric Pressure CVD of SnS and SnS₂ on Glass. *Chem. Vapor Depos.,* **1998,** 4, 222-225.

(28) Hibbert, T. G.; Mahon, M. F.; Molloy, K. C.; Price, L. S.; Parkin, I. P., Deposition of tin sulfide thin films from novel, volatile (fluoroalkythiolato)tin(iv) precursors. *J. Mater. Chem.,* **2001,** 11, 469-473.

(29) Price, L. S.; Parkin, I. P.; Hardy, A. M. E.; Clark, R. J. H.; Hibbert, T. G.; Molloy, K. C., Atmospheric Pressure Chemical Vapor Deposition of Tin Sulfides (SnS, Sn₂S₃, and SnS₂) on Glass. *Chem. Mater.,* **1999,** 11, 1792-1799.

(30) Gao, C.; Shen, H., Influence of the deposition parameters on the properties of orthorhombic SnS films by chemical bath deposition. *Thin Solid Films,* **2012,** 520, 3523-3527.

(31) Reghima, M.; Akkari, A.; Guasch, C.; Turki-Kamoun, N., Structure, Surface Morphology, and Optical and Electronic Properties of Annealed SnS Thin Films Obtained by CBD. *J. Elec Mater.,* **2014,** 43, 3138-3144.

(32) Gedi, S.; Minnam Reddy, V. R.; Park, C.; Chan-Wook, J.; K.T, R. R., Comprehensive optical studies on SnS layers synthesized by chemical bath deposition. *Opt. Mater.,* **2015,** 42, 468-475.

(33) Koteeswara Reddy, N.; Devika, M.; Ahsanulhaq, Q.; Gunasekhar, K. R., Growth of Orthorhombic SnS Nanobox Structures on Seeded Substrates. *Cryst. Grow. Des.,* **2010,** 10, 4769-4772.

(34) Mariano, A. N.; Chopra, K. L., Polymorphism in some IV-VI compounds induced by high pressure and thin-film epitaxial growth. *Appl. Phys. Lett.,* **1967,** 10, 282-284.

(35) Deng, Z.; Han, D.; Liu, Y., Colloidal synthesis of metastable zinc-blende IV-VI SnS nanocrystals with tunable sizes. *Nanoscale,* **2011,** 3, 4346-4351.

(36) Herron, S. M.; Tanskanen, J. T.; Roelofs, K. E.; Bent, S. F., Highly Textured Tin(II) Sulfide Thin Films Formed from Sheetlike Nanocrystal Inks. *Chem. Mater.,* **2014,** 26, 7106-7113.

(37) Patra, B. K.; Guria, A. K.; Dutta, A.; Shit, A.; Pradhan, N., Au-SnS Hetero Nanostructures: Size of Au Matters. *Chem. Mater.,* **2014,** 26, 7194-7200.

(38)Rabkin, A.; Samuha, S.; Abutbul, R. E.; Ezersky, V.; Meshi, L.; Golan, Y., New Nanocrystalline Materials: A Previously Unknown Simple Cubic Phase in the SnS Binary System. *Nano Lett.,* **2015,** 15, 2174-2179.

(39) Schneikart, A.; Schimper, H.-J.; Klein, A.; Jaegermann, W., Efficiency limitations of thermally evaporated thin-film SnS solar cells. *J. Phys. D: Appl. Phys.,* **2013,** 46, 305109.

(40) Minnam Reddy, V. R.; Gedi, S.; Park, C.; R.W, M.; K.T, R. R., Development of sulphurized SnS thin film solar cells. *Cur. Appl. Phys.,* **2015,** 15, 588-598.

(41) Ichimura, M.; Takeuchi, K.; Ono, Y.; Arai, E., Electrochemical deposition of SnS thin films. *Thin Solid Films,* **2000,** 361, 98-101.

(42) Cheng, S.; Chen, G.; Chen, Y.; Huang, C., Effect of deposition potential and bath temperature on the electrodeposition of SnS film. *Opt. Mater.,* **2006,** 29, 439-444.

(43) Steichen, M.; Djemour, R.; Gütay, L.; Guillot, J.; Siebentritt, S.; Dale, P. J., Direct Synthesis of Single-Phase p-Type SnS by Electrodeposition from a Dicyanamide Ionic Liquid at High Temperature for Thin Film Solar Cells. *J. Phys. Chem. C,* **2013,** 117, 4383-4393.

(44) Seal, M.; Singh, N.; McFarland, E. W.; Baltrusaitis, J., Electrochemically Deposited Sb and In Doped Tin Sulfide (SnS) Photoelectrodes. *J. Phys. Chem. C,* **2015,** 119, 6471-6480.

(45) Zainal, Z.; Hussein, M. Z.; Ghazali, A., Cathodic electrodeposition of SnS thin films from aqueous solution. *Sol. Energ. Mater. Sol. C.,* **1996,** 40, 347-357.

(46) Mathews, N. R.; Anaya, H. B. M.; Cortes-Jacome, M. A.; Angeles-Chavez, C.; Toledo-Antonio, J. A., Tin Sulfide Thin Films by Pulse Electrodeposition: Structural, Morphological, and Optical Properties. *J. Electrochem. Soc.,* **2010,** 157, H337-H341.

(47) Boudjouk, P.; Seidler, D. J.; Grier, D.; McCarthy, G. J., Benzyl-Substituted Tin Chalcogenides. Efficient Single-Source Precursors for Tin Sulfide, Tin Selenide, and Sn(SₓSe₁₋ₓ) Solid Solutions. *Chem. Mater.,* **1996,** 8, 1189-1196.

(48) Calixto-Rodriguez, M.; Martinez, H.; Sanchez-Juarez, A.; Campos-Alvarez, J.; Tiburcio-Silver, A.; Calixto, M. E., Structural, optical, and electrical properties of tin sulfide thin films grown by spray pyrolysis. *Thin Solid Films,* **2009,** 517, 2497-2499.

(49) Ray, S. C.; Karanjai, M. K.; Dasgupta, D., Structure and photoconductive properties of dip-deposited SnS and SnS₂ thin films and their conversion to tin dioxide by annealing in air. *Thin Solid Films,* **1999,** 350, 72-78.

(50) Sinsermsuksakul, P.; Sun, L.; Lee, S. W.; Park, H. H.; Kim, S. B.; Yang, C.; Gordon, R. G., Overcoming Efficiency Limitations of SnS-Based Solar Cells. *Adv. Energ. Mater.,* **2014,** 4, No. 1400496.

(51)Park, H. H.; Heasley, R.; Sun, L.; Steinmann, V.; Jaramillo, R.; Hartman, K.; Chakraborty, R.; Sinsermsuksakul, P.; Chua, D.; Buonassisi, T.; Gordon, R. G., Co-optimization of SnS absorber and Zn(O,S) buffer materials for improved solar cells. *Prog. Photovol.: Res. App.,* **2014,** 27, 901-908.

(52) Scragg, J. J.; Ericson, T.; Kubart, T.; Edoff, M.; Platzer-Björkman, C., Chemical Insights into the Instability of Cu₂ZnSnS₄ Films during Annealing. *Chem. Mater.,* **2011,** 23, 4625-4633.

(53) Ghosh, B.; Bhattacharjee, R.; Banerjee, P.; Das, S., Structural and optoelectronic properties of vacuum evaporated SnS thin films annealed in argon ambient. *App. Surf. Sci.,* **2011,** 257, 3670-3676.

(54) Devika, M.; Koteeswara Reddy, N.; Venkatramana Reddy, S.; Ramesh, K.; Gunasekhar, K. R., Influence of rapid thermal annealing (RTA) on the structural and electrical properties of SnS films. *J. Mater. Sci: Mater. Electron.,* **2009,** 20, 1129-1134.

(55) Hou, X.; Choy, K. L., Processing and Applications of Aerosol-Assisted Chemical Vapor Deposition. *Chem. Vapor Depos.,* **2006,** 12, 583-596.

(56) Wildsmith, T.; Hill, M. S.; Johnson, A. L.; Kingsley, A. J.; Molloy, K. C., Exclusive formation of SnO by low temperature single-source AACVD. *Chem. Commun.,* **2013,** 49, 8773-8775.

(57) Romero, M.; Huerta, L.; Akachi, T.; Llamazares, J. L. S.; Escamilla, R., X-ray photoelectron spectroscopy studies of the electronic structure of superconducting Nb$_2$SnC and Nb$_2$SC. *J. Alloys Compd.,* **2013,** 579, 516-520.

(58) See *JCPDS No. 00-039-0354*.

(59) Dennis, B. S.; Haftel, M. I.; Czaplewski, D. A.; Lopez, D.; Blumberg, G.; Aksyuk, V. A., Compact nanomechanical plasmonic phase modulators. *Nature Photon.,* **2015**.

(60) See *JCPDS No. 04-004-8426*.

(61) Burton, L. A.; Walsh, A., Phase Stability of the Earth-Abundant Tin Sulfides SnS, SnS2, and Sn2S3. *J. Phys. Chem. C,* **2012,** 116, 24262-24267.

(62) Patel, M.; Mukhopadhyay, I.; Ray, A., Molar optimization of spray pyrolyzed SnS thin films for photoelectrochemical applications. *J. Alloys Compd.,* **2015,** 619, 458-463.

(63) Nelson, J., *The Physics of Solar Cells*. Imperial College Press: London, 2003; Vol. 2.

(64) Foley, P.; Zeldin, M., Bis(dimethylamido)tin(II). Synthesis and characterization. *Inorg. Chem.,* **1975,** 14, 2264-2267.

(65) Olmstead, M. M.; Power, P. P., Structural studies of tin(II) and lead(II) dimethylamides: X-ray crystal structure of [Sn(NMe2)2]2 and isolation of its lead analog. *Inorg. Chem.,* **1984,** 23, 413-415.

(66) Fulmer, G. R.; Miller, A. J. M.; Sherden, N. H.; Gottlieb, H. E.; Nudelman, A.; Stoltz, B. M.; Bercaw, J. E.; Goldberg, K. I., NMR Chemical Shifts of Trace Impurities: Common Laboratory Solvents, Organics, and Gases in Deuterated Solvents Relevant to the Organometallic Chemist. *Organometallics,* **2010,** 29, 2176-2179.

TOC: (3.6 cm x 7.59 cm)